ARMY RESEARCH LABORATORY

Morphology of Extinguished Monolithic JA2 Grains Fired in a 30-mm Solid Propellant Electrothermal-Chemical (SPETC) Gun

Robert J. Lieb
Christopher J. Gillich

ARL-TR-606 November 1994

NOTICES

Destroy this report when it is no longer needed. DO NOT return it to the originator.

Additional copies of this report may be obtained from the National Technical Information Service, U.S. Department of Commerce, 5285 Port Royal Road, Springfield, VA 22161.

The findings of this report are not to be construed as an official Department of the Army position, unless so designated by other authorized documents.

The use of trade names or manufacturers' names in this report does not constitute indorsement of any commercial product.

REPORT DOCUMENTATION PAGE

Form Approved OMB No. 0704-0188

1. AGENCY USE ONLY *(Leave blank)*	2. REPORT DATE	3. REPORT TYPE AND DATES COVERED
	November 1994	Final - Sep 93 - Jan 94

4. TITLE AND SUBTITLE

Morphology of Extinguished Monolithic JA2 Grains Fired in a 30-mm Solid Propellant Electrothermal-Chemical (SPETC) Gun

5. FUNDING NUMBERS

PR: 1L161102AH43

6. AUTHOR(S)

Robert J. Lieb and Christopher J. Gillich

7. PERFORMING ORGANIZATION NAME(S) AND ADDRESS(ES)

U.S. Army Research Laboratory
ATTN: AMSRL-WT-PD
Aberdeen Proving Ground, MD 21005-5006

8. PERFORMING ORGANIZATION REPORT NUMBER

9. SPONSORING/MONITORING AGENCY NAMES(S) AND ADDRESS(ES)

US Army Research Laboratory
ATTN: AMSRL-OP-AP-L
Aberdeen Proving Ground, MD 21005-5066

10.SPONSORING/MONITORING AGENCY REPORT NUMBER

ARL-TR-606

11. SUPPLEMENTARY NOTES

12a. DISTRIBUTION/AVAILABILITY STATEMENT

Approved for public release; distribution is unlimited.

12b. DISTRIBUTION CODE

13. ABSTRACT *(Maximum 200 words)*

Monolithic grains of JA2 were fired in a 30-mm solid propellant electrothermal-chemical (SPETC) gun and were recovered after self- extinguishing because of depressurization. A morphological investigation was performed on these grains to gain insight into the interaction between the plasma and the propellant.

Scanning electron microscopy (SEM) was used to characterize the morphology of the combustion surface and bulk of the propellant. Results show that the propellant burning surface was pitted and showed evidence of both brittle fracture and plastic flow. These features were the results of rapid pressurization within the single perforated grain caused by the plasma injection and the subsequent burning. Regions within the propellant showed evidence of augmented mass generation when compared with conventional propellant combustion. Mechanisms causing this accelerated burning are conjectured; they included erosive burning, fracture-generated tunneling, and in-depth burning. Micrographs are presented to support these findings and proposals are made to exploit these enhanced burning processes.

14. SUBJECT TERMS	15. NUMBER OF PAGES
SPETC, ETC, JA2, Gun Propellants, Morphology, Extinguished	29
	16. PRICE CODE

17. SECURITY CLASSIFICATION OF REPORT	18. SECURITY CLASSIFICATION OF THIS PAGE	19. SECURITY CLASSIFICATION OF ABSTRACT	20. LIMITATION OF ABSTRACT
UNCLASSIFIED	UNCLASSIFIED	UNCLASSIFIED	UL

Intentionally Left Blank

ACKNOWLEDGMENTS

The authors thank the following people who contributed to this report. Their efforts and the information that they shared significantly increased the value of the report.

First we wish to extend thanks to Hugh McElroy of Olin Ordnance Corporation who had initially fired the monolithic charges under Olin 1061 Alternate Electrothermal-Chemical Propellants contract. He generously brought his observations to our attention, and made samples and firing records available for study. In addition, thanks go to Lee Harris, COR for contract 1061 from Picatinny Arsenal, for reading initial drafts of this report and for providing valuable comments concerning the experimental set-up of the 30-mm firings.

Thanks are due to Kevin White of the Army Research Laboratory. He offered suggestions to clarify and relate some concepts dealing with conventional ignition in the 30-mm gun and provided extinguished specimens from those 30-mm firings. Thanks also to Fred Robbins, ARL, for his help and advice concerning the nature and accuracy of interior ballistic code predictions (IBHVG2).

A special thanks is given to Rose Pesce-Rodiriguez, ARL, for her skills with the Fourier transform infrared (FTIR) microscope which was used to detect the decomposition products below the combustion surface of the SPETC extinguished propellant. We extend many thanks to her for allowing us to use her unpublished results.

The reviewers, Arpad Juhasz (ACOR for the 1061 contract) and Bill Oberle, ARL, are thanked for suggestions and corrections that made the manuscript more pertinent and readable.

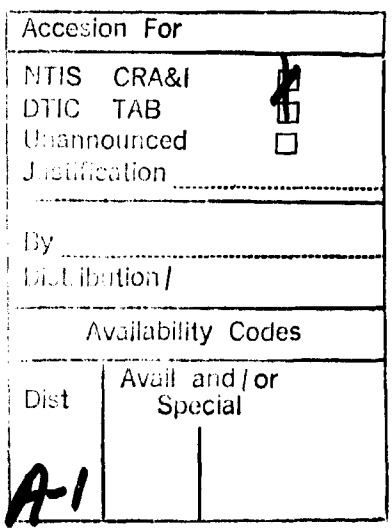

Intentionally Left Blank

TABLE OF CONTENTS

Intentionally Left Blank

LIST OF FIGURES

Intentionally Left Blank

1. INTRODUCTION

One of the hopes of the solid propellant electrothermal-chemical (SPETC) propulsion concept is to regulate the mass generation within the gun by using a plasma to control the generation of surface area and to augment the burning of the solid propellant charge. Investigation of the morphology of extinguished surfaces of monolithic JA2 grains that were fired in a 30-mm SPETC gun has shown evidence of augmented burning. There were also indications of new surface area generation caused by mechanical inhomogeneities within the propellant.

The monolithic JA2 grains were fired in a test series[1] that used various amounts of propellant and an ignition source that included a range of plasma-generating voltage pulses. These firings showed enhanced performance (i.e., higher projectile velocities than predicted with a standard interior ballistics code). This extra performance was initially attributed to erosive burning that was thought to augment or enhance the burning *rate* of the propellant. However, there was evidence collected on residual propellant grains, recovered after the firings, that fracture and unusual burning patterns could have contributed extra surface area. (See summary of section 3.7 on page 11.) This would explain the enhanced performance without necessarily increasing the burning rate of the propellant by creating additional surface area, thereby accounting for the accelerated mass generation during combustion. To help resolve the mechanism responsible for the increased performance, the residual grains (rapidly extinguished grains remaining after bullet exit) were delivered to ARL for morphological investigation using scanning electron microscopy (SEM). The resulting micrographs provide evidence of the processes occurring during combustion.

In this study, comparisons are made between extinguished grains from SPETC firings and extinguished propellant from low pressure combustion. Propellant subject to conventional ignition sources are also included in this comparison. Recommendations are made for additional investigation.

2. BACKGROUND DETAILS

A series of SPETC firings had been performed in a 30-mm gun using monolithic JA2 charges.[1] Information pertinent to this study is provided below.

The basic gun configuration is presented in Figure 1. The monolithic charges were made of a single right-circular cylinder with one center perforation. These grains were ignited with a plasma pulse produced by various combinations of high voltage and current duration applied to a nonenergetic material. The plasma was introduced into the perforation by an injector that intruded a short way into the base of the grain. The charge consisted of either a full, three-quarter, half, or quarter grain with dimensions and mass, as listed in Table 1.

The performance predictions for this gun with the various charge masses were produced using IBHVG2 (Interior Ballistics of High Velocity Guns Version 2), an interior ballistic code.[2] By using the gun parameters, such as the charge weight and dimensions, propellant thermochemistry, chamber volume, barrel length, projectile mass, etc., and assuming conventional combustion using established propellant burning rates for JA2, the velocities, chamber pressures, percentage of the charge consumed at any time can be predicted. When applied to untested conventional systems, IBHVG2

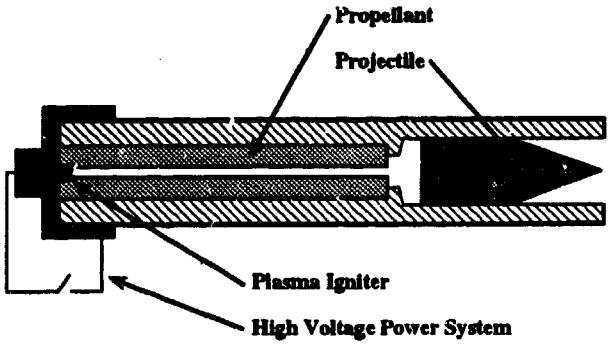

Figure 1. Schematic Diagram of the 30-mm SPETC Gun.

Table 1. Monolithic Propellant Dimensions

Diameter = 28.1 mm Web = 11 mm Perforation Diameter = 6.1 mm		
Charge (cm)	Length (mm)	Mass (g)
Quarter	46	45
Half	91	86
Three-Quarters	140	130
Full	190	180

predictions are usually within 5 % of subsequent experimental results.[3] If the code is used on well-known systems where only the projectile mass, the charge weight, or a combination of a few such parameters is varied, the predictions are good to within a few percent.

The predicted values of peak pressure and projectile kinetic energy are presented in Table 2 for each charge weight. (Electric power curves were included in these predictions.) Also included in the table are these measured values from the 30-mm firings along with the peak electric power supplied to generate the plasma, and the total electric energy delivered during the plasma generation. These values are graphically illustrated in Figures 2 and 3 and are included here for reference. Detailed discussion of these results is presented in Reference 1.

Many test configurations and procedure modifications were used during this test series. The initial test configuration produced evidence of enhanced performance that may have been attributable to fracture caused by expansion of the monolithic charge. The experiment was modified to reduce this fracture by adding a thin sleeve inside the center perforation (moderator case). The force of the plasma against the perforation wall was diminished and fracture was reduced, but so was the performance. Indications of radial fracture persisted, so an outside steel case was introduced to eliminate increased mass generation caused by conventional fracture. The steel sleeve stopped evidence of conventional fracture and helped elucidate the mechanism responsible for the added performance. IBHVG2 was then used in an attempt to match the SPETC gun performance by introducing additional mechanisms (erosive and ablative) to account for the augmented pressurization rates. The code predictions were finally brought into fair agreement with test results through these assumptions, but the actual mechanism of augmentation, while conjectured, was unresolved.

To resolve the nature of the augmentation mechanism, the morphology of the residual grains from the above test series was investigated to uncover evidence that would indicate the process of augmentation.

3. PROCEDURE AND RESULTS

The residual grains from the firing series were received and are indicated by shading in Table 2. All these grains and several virgin grains were thoroughly inspected. The following descriptions are the result of intensive investigation of more than 400 micrographs. All evidence for features uncovered

Table 2. Maximum Pressure and Velocity Values from 30-mm SPETC Firings

Shot	Charge	Maximum Pressure (MPa)	Projectile KE (kJ)	Peak Power (MW)	Electric Energy (kJ)
Predicted					
NA	Quarter	14	3.5	0	0
NA	Half	41	8.1	0	0
NA	Full	90	18.4	0	0
Experimental					
No Case					
1	Quarter	67	17	16	30
5	Quarter	67	12	15	15
7	Quarter	74	19.2	30	29
9	Quarter	47	6.1	12	8
2	Half	120	38	33	58
6	Half	110	25	30	28
8	Half	130	31	60	54
10	Half	110	11	22	15
Moderator Case *(Inside Perforation)*					
11	Quarter	34	4.4	32	30
14	Quarter	130	7.9	47	30
12	Half	120	21	55	54
13	Half	40	22	31	57
Steel Case *(Outside Grain)*					
21	Half	34	10	18	30
22	Half	110	63	35	57
23	Half	110	57	25	45
24	Half	27	4.9	10	18
25	Half	34	9.5	19	30
26	Half	40	16	15	15
27	Half	120	45	29	27
40	Full	180	57	17	31
41	Full	380	90	35	57
42	Full	250	81	55	83

cannot be presented. However, significant findings will be illustrated and supported as much as possible. All illustrations of general features show specific results that are typical.

3.1 Specimen Preparation. The grains were fired and rapidly extinguished because of the pressure drop at bullet exit. When the gun pressure is reduced in this manner, the flame is rapidly expanded away from the surface. The heating and pyrolyzing of surface material is very rapidly reduced, and combustion stops. How quickly this occurs is not exactly known. However, from previous studies

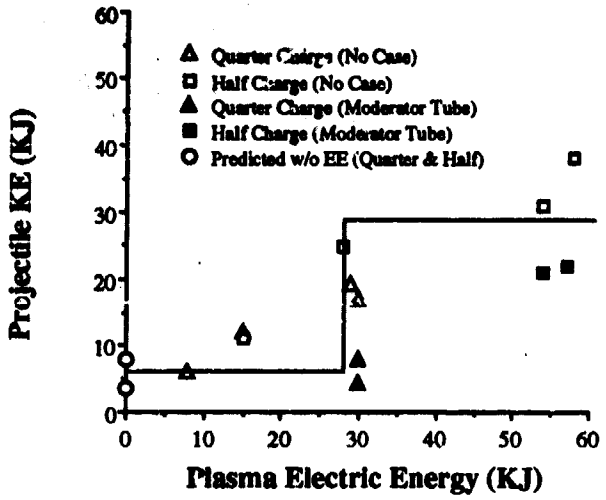

Figure 2. Plasma Energy vs Projectile Kinetic Energy for Early Firings

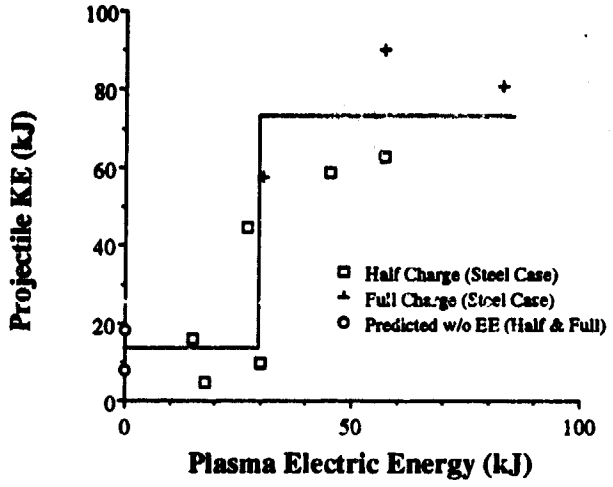

Figure 3. Plasma Energy vs Projectile Kinetic Energy for Steel Case Firings

with extinguished rocket propellant[4] and more recent studies with extinguished gun propellant,[5,6] the process has been shown to be very rapid and the morphology of the extinguished surfaces has been shown to provide information that can be directly linked with the surface structure during propellant combustion. Combustion models have been generated using the uncovered information and it seems likely that many of the structural features from the gun environment are preserved. The specimens were received for morphological investigation as they had been collected at the gun site.

A major concern in specimen preparation is to avoid producing artifacts (morphological features caused by the preparation method) that could be mistaken for intrinsic features. All the grains were carefully dusted to remove loose debris from the surface and then optically photographed. After careful planning, it was decided to cold-fracture[7] each specimen along the grain axis to reveal the burned perforation surface, the unburned web, and the thermal transition region between. To ensure controlled fracture, it was necessary to cut the longer specimens into 2 to 3-cm sections by sawing perpendicular to the grain axis. Grains were then cold fractured after careful selection of fracture initiation sites. Schematic diagrams of these operations are illustrated in Figure 4. The specimens were mounted, sputter coated, and placed within the SEM. Details of these operations are provided in Reference 7.

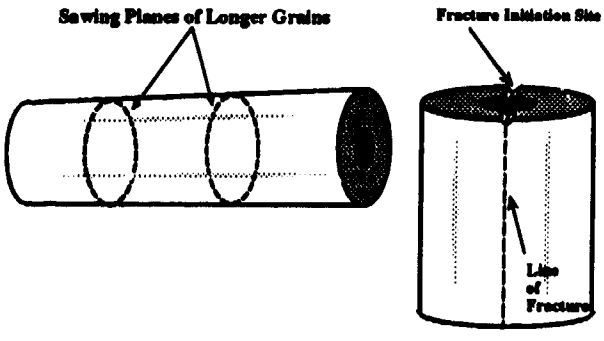

Figure 4. Sectioning of the SPETC Specimens

3.2 Undamaged JA2. Figure 5 shows micrographs of the cold-fractured surface of a virgin grain prepared in the same fashion as the extinguished specimens and is presented as a basis for comparison. Figure 5a shows that the typical JA2 cold-fracture surface is smooth, indicating brittle fracture. Some nitrocellulose (NC) is observed because the high nitration level (13.1%)

a. Fracture Surface (≈1000X)

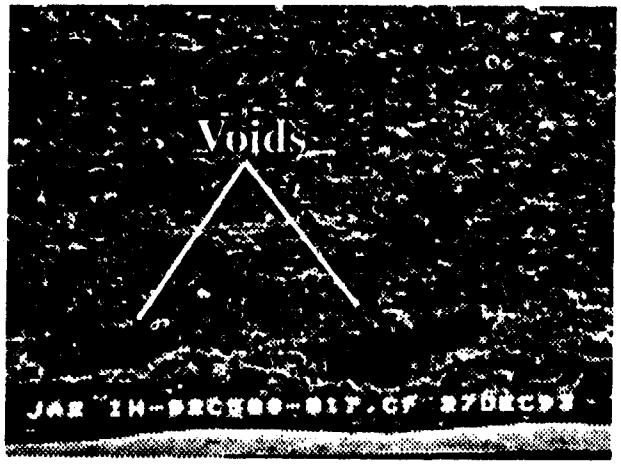

b. Voids near Center Perforation (≈50X)

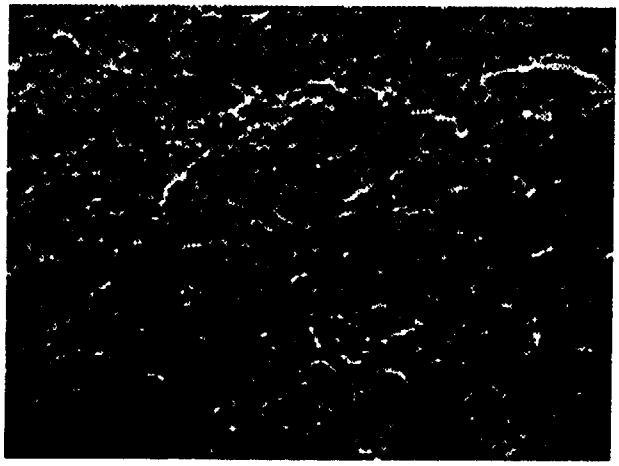

c. Perforation Surface (≈200X)

Figure 5. Virgin JA2 Grain

of the NC prevents all the fiber from dissolving in the plasticizer. Other propellants that use lower levels of nitration (12.6%) have the NC completely dissolved and do not show exposed fibers. The only other notable feature in typical JA2 propellant is the presence of very small (0.5 to 2 μm) particles distributed throughout the propellant. Their identity has not been established. They could be very fine carbon black, which is an added ingredient, or they could be small particles of MgO that are added as a lubricant to aid in the extrusion process. In any case, these small particles seem to occur throughout the material. The only defect appearing in these grains is shown in Figure 5b. A series of large (200 to 400 μm) voids, apparently caused by shearing during extrusion, was found very near the perforation surface. These voids should affect only the very early burning of the grain and were not believed to affect the morphology of the extinguished specimens. The inside perforation surface, shown in Figure 5c, was very smooth and featureless.

3.3 Residual Grains with No Case. In all micrographs appearing in this report, unless otherwise noted, the plasma was injected on the right and the projectile moved to the left. The general flow of generated gases then was to the left. There were situations in which the flow of gas was in other directions. These will be noted.

The initial 10 firings were done with no supporting encasement for the grains. The grain diameter was 28.1 mm and the gun bore diameter was 30 mm. This left about 0.9 mm of clearance between the outside of the grain and the inside of the chamber, if the grain was centered. The plasma entered the perforation at very high temperature (~10^4 K) and pressure. This resulted in rapid expansion of the grain to the confining walls. At room temperature and normal deformation rates, JA2 deforms plastically within the gun. However, it is known that at lower temperatures or higher rates, the mechanical response of

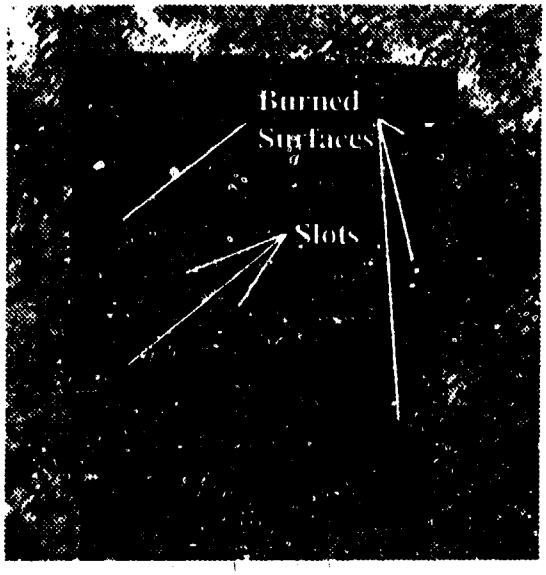

Figure 6. A No-Case Residual Grain (Optical)

JA2 becomes more brittle.[8,9] At strain rates of 100 s^{-1}, brittleness begins at about -20° C. This transition temperature increases by about 12° C for every decade of rate increase. Figure 6 shows the appearance of the residual grain from Shot Number 8 and is typical of the features of the caseless firings. The two exposed web surfaces are *not* fracture surfaces. They were combustion surfaces and were similar to the surfaces in the slots within the perforation and on the cone at the left of the picture. They were most likely the result of radial fractures that occurred upon expansion. The flame followed this fracture tip and ignited the newly exposed surface soon after it was created. This accounts for some of the increased performance in this firing series.

The cone surface was serrated or scalloped as a result of an apparent scooping or other rapid burning process. To various degrees, this was a common feature of all combustion surfaces. A typical formation is shown in Figure 7. The edge of the cone appears on the right and the scalloping began on the edge and continued to the outer edge of the grain. Debris can be seen on the leeward side of the depressions, and small particles, which seem to be fused to the surface, were distributed uniformly across the surfaces.

3.4 Residual Grains with Moderator Case. It was recognized from the appearance of the caseless grains that fracture may have been a problem.[1] However, it was also recognized that the additional area presented to the flame because of cracks such as these would have to be much more numerous to explain the increased mass generation rate. Therefore, the experimental procedure was modified by adding a thin moderator tube to the inside perforation surface. The function of the tube was to moderate the plasma blast so that grain fracture was reduced. Fracture was reduced at the expense of performance, but it was not eliminated. Two of the three residual grains using this modification showed a single slot similar to the many slots found in the No-Case configuration. Figure 8 shows a split moderator-case residual grain. The web in the center of the figure was exposed by cold fracture after recovery. The web at the top and bottom of the figure was burned-through during the firing. Clearly, the case helped reduce fracture, but as can be seen from Figure 2, the performance was markedly reduced. However, the performance was still greater than predicted, indicating another pressure-augmentation mechanism at work.

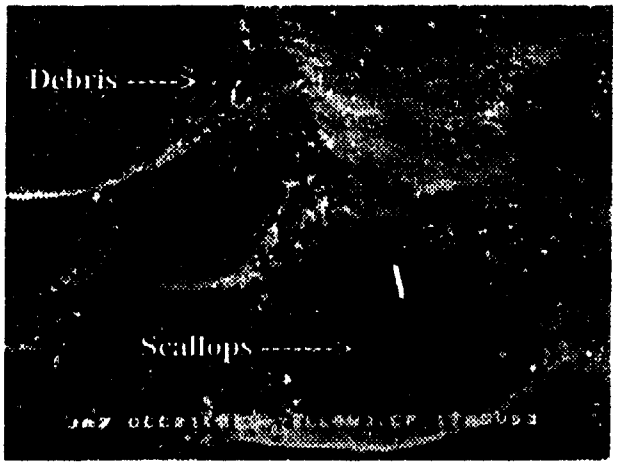

Figure 7. The Beginning of Scalloping, Forming the Cone (≈50X)

Figure 9a is a magnified view of the white rectangular region shown in Figure 8 and shows the first evidence of what has been termed "in-depth" burning. The significant aspects of this micrograph are the depth of the intrusion, the sharp line of demarcation between burned and unburned regions, and the isolation of some combustion zones (dashed rectangle). This implies that a process was active that directed ignition into specific regions. Figure 9b shows a much more magnified view of 9a (within the white circle) that shows that this boundary separation is maintained even on a small scale.

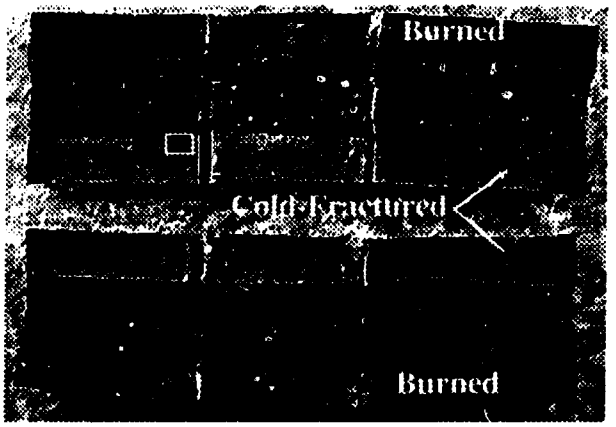

Figure 8. A Split Moderator-Case Residual Grain (Optical)

3.5 Residual Grains with Steel Case. The remaining firings were all conducted using a steel case confinement. The case was effective in eliminating slots as those observed previously, as long as the electrical energy remained below about 30 kJ. This is the case for Shots 21, 24, 25, and 40. In each of those instances, it appears that the case had sufficient strength to prevent radial fracture. This was not the true for shots 41 and 42. The elevated electrical energies may have produced conditions that again caused the radial fracture.

Many interesting features were found in the steel case grains. Figure 10a shows the cold-fractured residual grain from Shot 21. This grain showed the scalloping and combustion surfaces like the other grains, and erosive or ablative burning which is indicated by the larger inner diameter at the plasma entrance (on the right) and at the combustion product exit (on the left). These regions contain gaseous and plasma mixtures traveling at high velocity. The plasma is injected at very high speeds and at high temperature causing erosion of the perforation at the entry. As combustion occurs within the perforation, the generated gasses flow to lower pressure regions behind the projectile base. This causes erosion at the other end of the grain as the hot gasses exit at high velocity. This erosive-ablative process contributes to the mass generation augmentation and was a common feature in all the steel case firings.

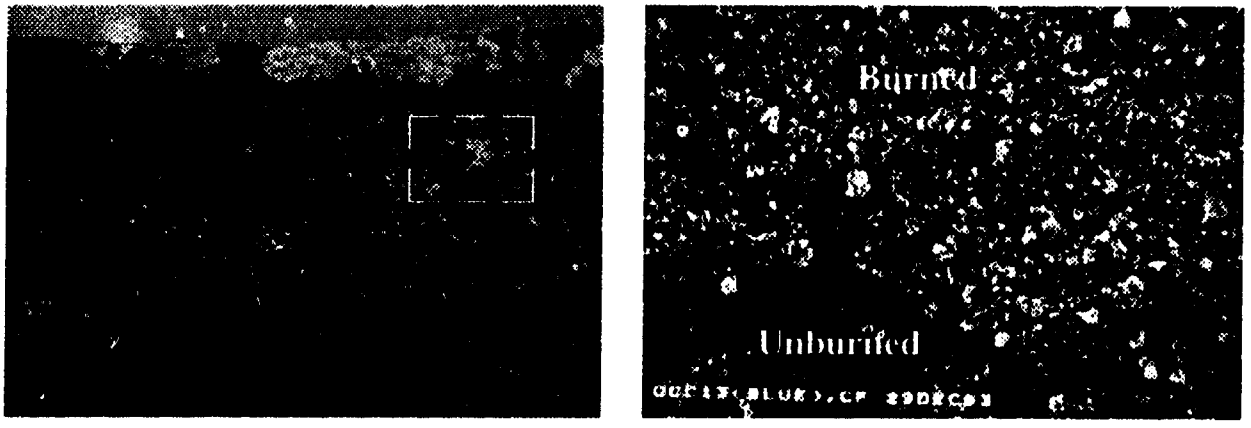

a. ≈ 15X b. ≈ 400X

Figure 9. Cold Fractured Web Surface from the White Rectangle of Figure 8 Showing In-Depth Burning

The grain in Figure 10a showed another very unusual feature, a long tunnel-like structure along the top of the grain which extended more than 30 mm from the rear. At first it was believed to be a very long void. Upon closer examination, the walls of the tunnel were found to be combustion surfaces. This was puzzling since no voids observed in any extinguished grains before this study had ever been found with combusted interior surfaces. Figure 10b shows the region in the white rectangle of Figure 10a. It contains the tip of the tunnel and appears to have two precursor cracks in front of the tunnel. It seems as if cracks were formed by some mechanism (local high pressure) and then flame followed the cracks to extend the travel. This could be a mechanism similar to the radial cracks observed earlier in the no-case and modified-case firings. In those instances, the fracture proceeded in the radial direction, and then the high pressure plasma followed and ignited the fracture surface. Here, the crack followed an internal flaw in the axial direction and the plasma (or high pressure gas) penetrated into the surface to follow and provide impetus to extend the fracture. The taper of the perforation indicates that the rear (right) portion ignited earlier than the tip (left). The steel case supported the grain and prevented the crack from running to the outside. This permitted the crack to follow the internal flaw or inhomogeneity.

Other tunnel-like structures were discovered and appeared similar to the one discussed. The tunnel identified in Figure 10a as "Another Tunnel" is shown in Figure 11a. This micrograph shows the tip of the tunnel that was found just entering the middle section on the "floor" of the perforation (Figure 10a, white circle). The tunnel seems to have broken the surface just as the extinguishment took place. Figure 11b is a magnification of the tip region and shows debris on the rim of the intersection of the perforation and tunnel. This debris appears in the process of being pushed out of the tunnel and into the perforation. It is difficult to know the time that these features were frozen in place, but when they were, the flow of gas was out of the tunnel. It seems likely that combustion had been occurring within the tunnel as in the tunnel discussed above.

These processes indicate some penetration mechanism that caused combustion to occur beneath the surface, as observed in Figure 9. All residual grains were searched for evidence of subsurface burning, especially steel-case shots in which the performance was very high (the 40, 41, and 42 series). A micrograph of the residual grain from Shot 42 appears in Figure 12 and shows a region of contrasting surfaces. To more fully understand the combustion surfaces and their morphologies, a short discussion of combustion surfaces follows.

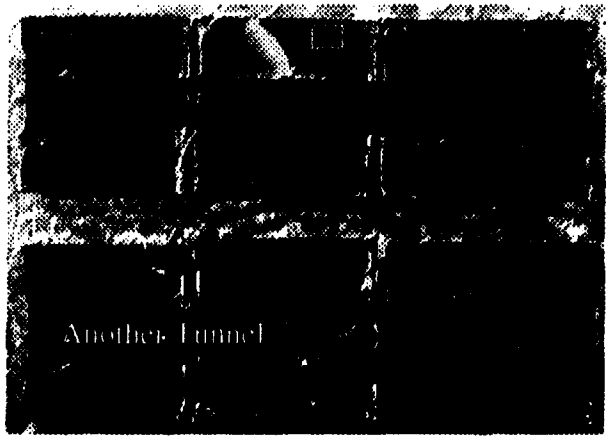

a. Whole Split Grain (Optical)

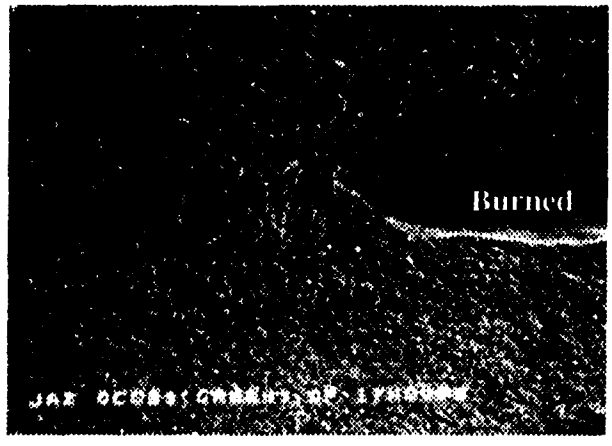

a. Tip of Tunnel (≈ 40X)

Figure 10 A Cold-Fractured Steel-Case Residual Grain

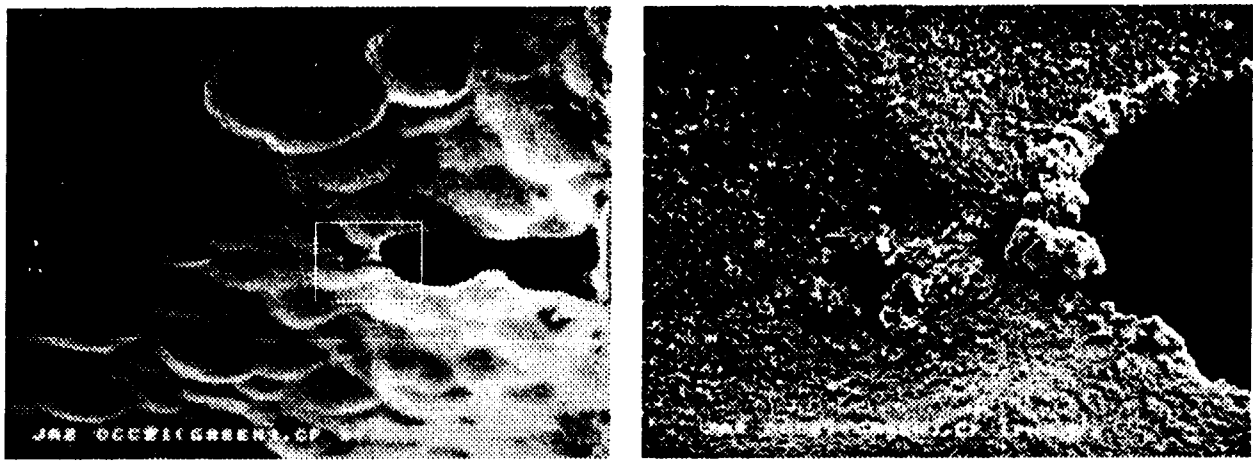

a. ≈ 15X b. ≈ 80X

Figure 11. Another Tunnel Emerging into the Perforation of the Residual Grain Shown in Figure 10

3.6 Morphology of Combustion Surfaces. Some combustion surfaces have already been presented. Figure 7 shows an extinguished perforation surface. At a magnification of 50, the surfaces appear smooth. If higher magnifications are viewed, as in Figure 13, the surfaces appear as the in-depth burned surfaces in Figure 9. The same is seen in Figure 11 at higher magnifications. How these surfaces compare with non-SPETC combusting JA2 is shown in Figure 14. These surfaces were the result of extinguishment at low and high pressure. The low pressure surface was a grain ignited at atmospheric pressures and extinguished with a chlorofluorocarbon jet. The high pressure surface was extinguished after conventional ignition in a 30-mm gun. These surfaces show a smooth surface that is probably the frozen melt surface of the JA2 with voids that are caused by residual decomposition during the rapid cooling. The high pressure surface has much smaller voids as expected and indicates that the cooling occurs at high pressure and very rapidly.

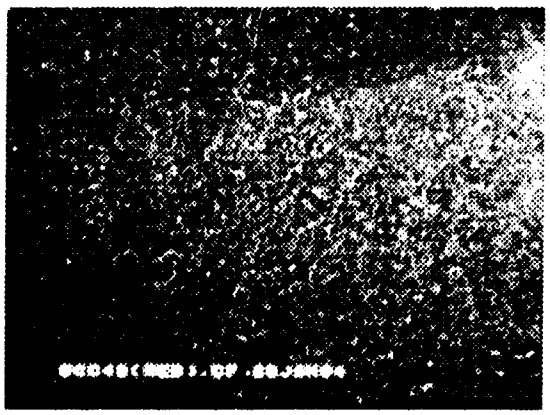

Figure 12. The Cold-Fractured Surface of the Web of the Residual Grain from Shot 42 Showing In-Depth Burning (≈ 15X)

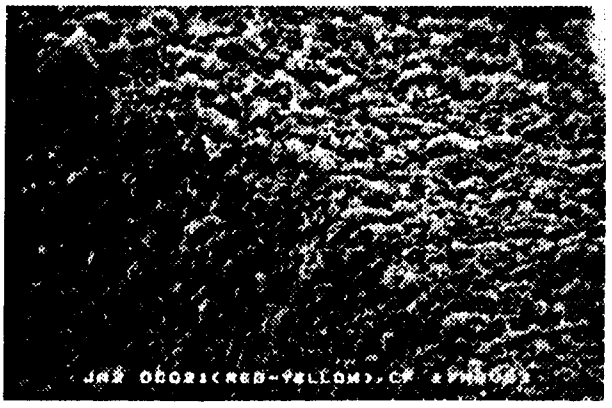

Figure 13. Detail of Figure 7 Showing the Rough Surface Appearance at Higher Magnification (≈ 350X)

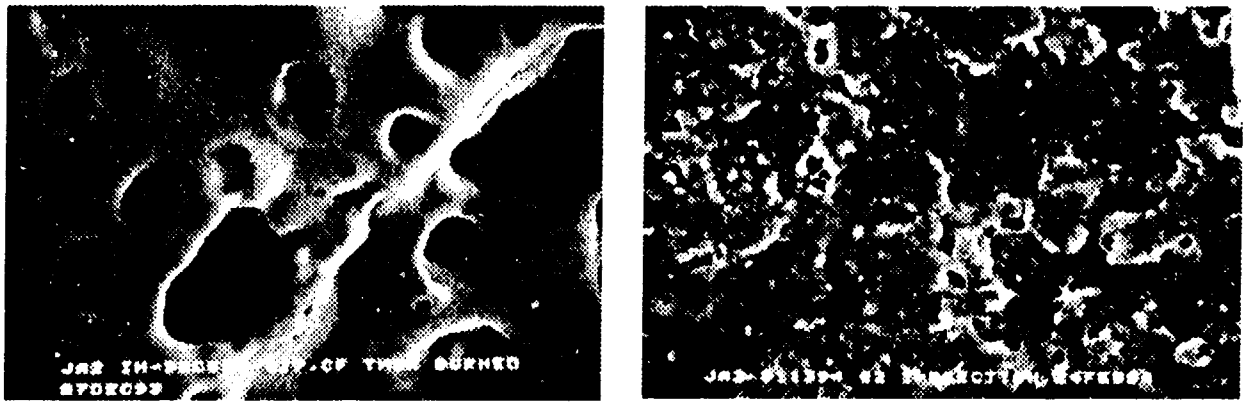

a. Low Pressure (≈ 350X) b. High Pressure (≈ 350X)

Figure 14. Extinguished JA2 Surfaces

These features are in contrast to the combustion surfaces mentioned for Figures 9, 11, and 13. The rough appearance at the corresponding magnifications indicates very little melting. An ablating or micro-deconsolidation process would account for the appearance of these exterior combustion surfaces.

3.7 In-Depth Burning. Using the previous section as background, the in-depth burning evidence can be more meaningfully discussed. The cold-fracture surface presented in Figure 5a was unburned and shows the intrinsic morphology of a fracture surface. The surface in Figure 15 is a detail from Figure 12, a mid-web fracture surface. It was smooth and the voids were small. Surfaces such as these were found in the cold-fractured webs of all shots in the 40 series. Taken all together, the previous information indicated subsurface or in-depth combustion. To confirm that combustion had taken place, each surface where the morphology suggested decomposition was scanned with surface microreflectance FTIR.[10] Typical spectra are presented in Figure 16. The top line is the spectrum of an NC standard film and shows two characteristic (stretching) peaks, NO_2 at 1650 cm^{-1} and C-O at 1270 cm^{-1}. The second line is web material from a virgin JA2 monolithic grain that was cold-fractured and shows that the surface was mostly NC. The third line is the spectrum taken from an

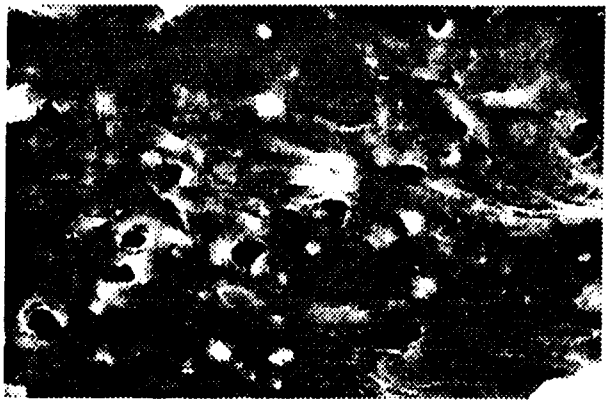

Figure 15. Detail of Figure 12 showing Evidence of In-Depth Burning (≈ 1000X)

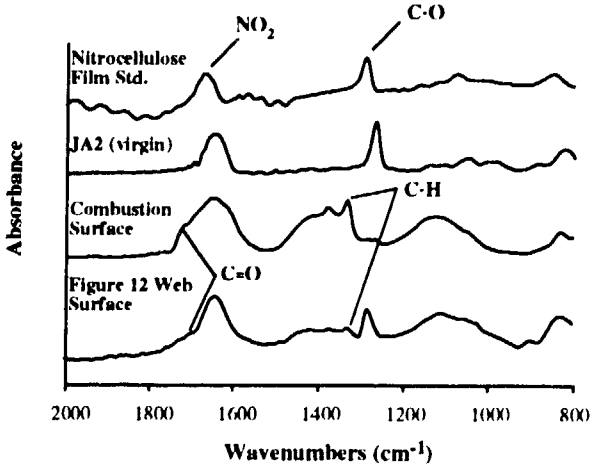

Figure 16. Surface Microreflectance FTIR Spectra Identifying Subsurface Decomposition

exposed extinguished surface. Decomposition is indicated by the broadened peak near 1650 cm^{-1}, the new peaks at 1720 (C=O), 1280, and 1330 (C-H) cm^{-1}, and the disappearance of the peak at about 1270 cm^{-1}. The broadening and the appearance of new peaks is consistent with the indicated bonds from carbonyl and aldehyde groups, which form during decomposition of NC. The last spectrum is the web area from the grain shown in Figure 12. The region from which this surface was taken was very far from the combustion surface. Although the surface was not as strongly degraded as the exposed combustion surface, this spectrum clearly shows signs of significant combustion. In-depth burning has been confirmed.

Among the more than 400 micrographs taken, many showed evidence of *unusual* combustion. There was evidence of erosive burning in regions of expected high-velocity gas flow, as indicated by the formation of cones from the center perforation in many of the residual grains. In other cases, channels were formed within the grain web as the high pressure gases and plasma made their way to lower pressure regions within the chamber (Figure 17a). Paths were also discovered to the outside of the grain around retaining hardware and other fixtures (the plasma injector in Figure 17b). The arrows in Figure 17 indicate the apparent paths taken by the gases to the outside. It seems as if there is evidence of new methods of gas generation, tunneling, and erosive burning, which directly, and indirectly, add to the generation of propelling gases. Indirectly, because the tunneling feature creates new area that continues to burn. In all areas directly exposed to the plasma, the ablative burning described earlier was evident. In regions sheltered from direct plasma exposure, evidence of burning similar to what was considered normal was found. These new burning processes, if exploited properly, may provide methods to improve gun performance.

3.8 The Melt Layer. The melt layer is the transition region observed in all extinguished propellant specimens preceding this study.[6] The layer begins at the combustion surface and extends toward the interior. It is characterized by a frozen appearance in which there is intimate contact between propellant components, and binder-filler interfaces are much less distinct as a result of partial melting. The layer extends from the surface to some depth where the propellant morphology becomes indistinguishable from its initial state. This transition is sometimes very abrupt and

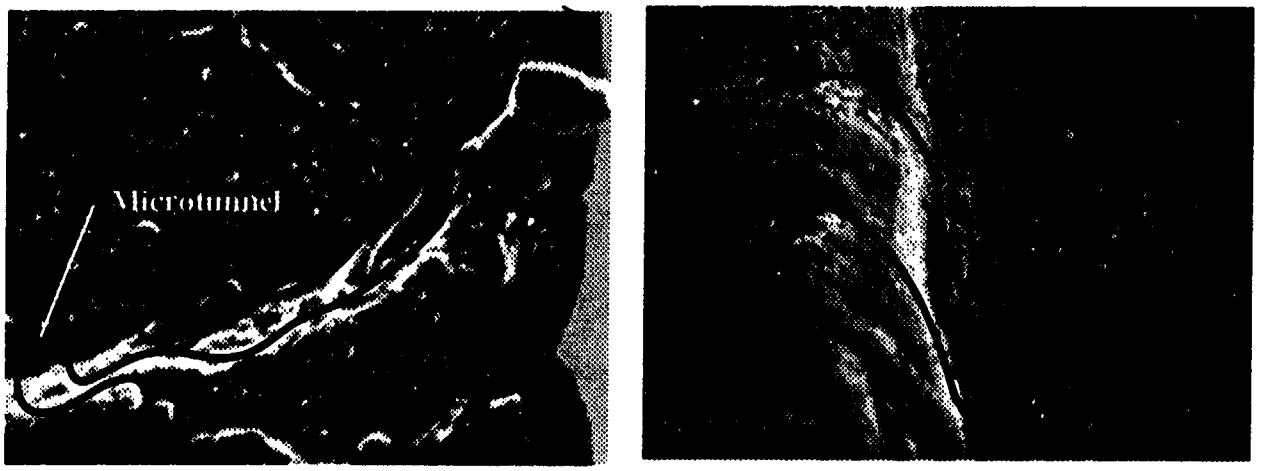

a. Microtunneling and Erosive Flow (≈ 200X) b. Erosive Flow around Plasma Injector (≈ 60X)

Figure 17. Micrographs Showing Evidence of Unusual Burning

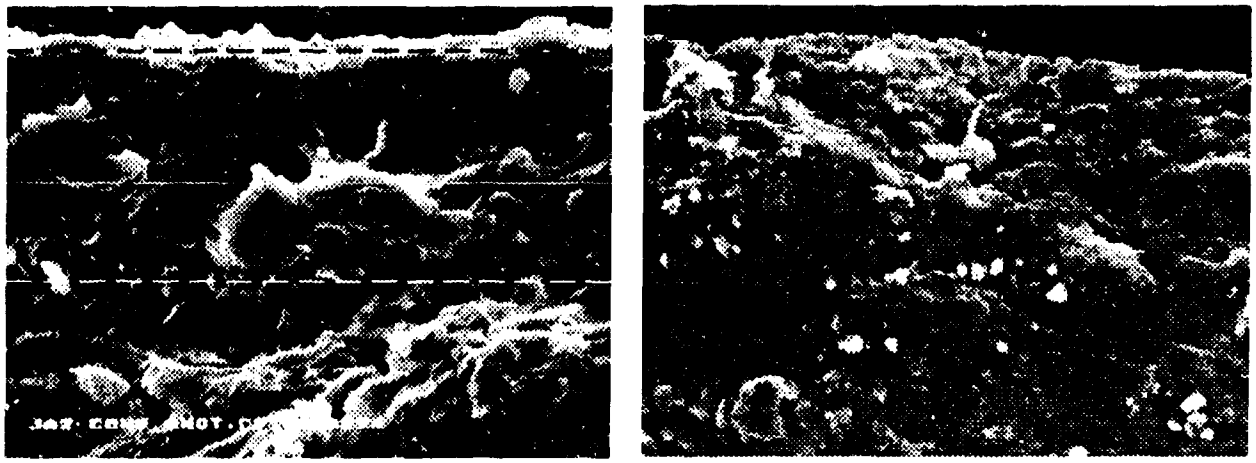

a. Extinguished at 140 MPa, Conventional Ignition (≈800X)

b. Extinguished at 95 MPa, SPETC Ignition (≈800X)

Figure 18. Thermal Layers for JA2 Propellant

sometimes more gradual. In most propellant melt layers studied by the authors, the thickness ranges between 15 and 40 μm. The melt layer is caused by heating during combustion that melts and pyrolyzes the surface. The depth of the layer is affected mostly by the burning rate. Higher burning rate propellants have thinner melt layers, as expected because of the shorter exposure time the surface has for thermal diffusion. This means that propellants with higher intrinsic burning rates have generally thinner thermal layers. Also, as pressure increases during combustion, the melt layer becomes thinner, mostly caused by higher burning rates at higher pressures.

JA2 burning rates are higher than those measured in most other gun propellants.[3] Therefore, thinner melt layers are expected. Figure 18a shows the thermal layer of JA2 propellant, ignited with a conventional ignition system in a 30-mm gun.[11] The residual propellant was extinguished after a maximum pressure of 140 MPa. The thickness of the melt layer in this specimen lies between 22 and 40 μm (as indicated by the lines). This thickness was a little greater than expected, but the gun pressures were low. JA2 grains fired in large caliber guns at higher pressures would be expected to have thinner melt layers. The micrograph in Figure 18b is of an SPETC monolithic grain fired in this series and extinguished after a maximum pressure of 95 MPa. It appears as if there was no melt layer at all. All features are sharp with distinct interface boundaries all the way from mid-web to the combustion surface, and none of the flowing appearances usually present in melt layers is seen. However, in the series of micrographs that led to Figure 18b, a 150-μm band extending from the surface was seen. This region is shown in Figure 19. (The

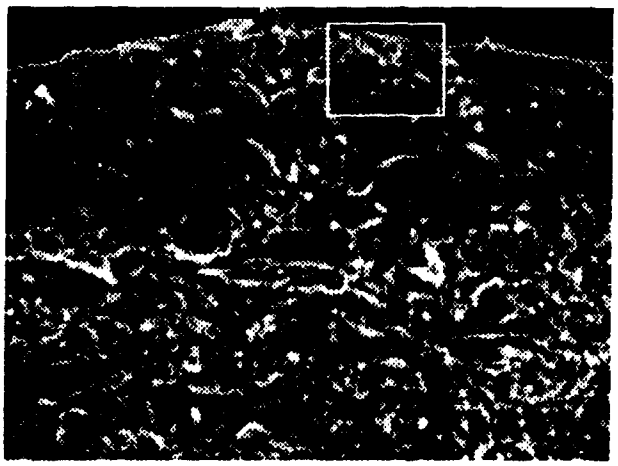

Figure 19. Expanded View of Figure 18b Showing the 150 μm Dark Band (≈200X)

white rectangle indicates the location of Figure 18b.) The process that produced the band formation has not been determined, but it was clearly a different process from what was observed in extinguished propellants that have undergone normal ignition. Severely erosive or ablative burning is indicated in the SPETC firings. Further study is required to confirm the mechanism responsible for these features.

4. ANALYSIS AND SPECULATIONS

Evidence cited demonstrates that processes occurred in these 30-mm SPETC gun firings that do not occur at significant levels during conventional propellant combustion. Efforts to determine the effect of plasma on the closed bomb burning rate have been inconclusive because of questions concerning the physical interaction of the plasma and propellant. Some studies indicate that there is no augmentation of the burning rates,[1] and other studies, currently under way, indicate significantly augmented mass generation.[12] From the results presented here it seems that the mechanisms that augment mass generation have a greater or lesser likelihood depending on the initial and ensuing conditions within the gun. Stated another way, the nature of interactions that occur between the plasma and the propellant is a strong function of the initial system configuration. From the no-case firings, it can be concluded that radial cracking can be induced, causing additional surface area. The introduction of moderator and steel cases reduced radial cracking and reinforced the confinement within the perforation. The increased confinement may have "turned on" or better enabled other processes that amplify the mass generation rate. This is indicated in Figures 2 and 3 by the step increases in performance at 30-kJ plasma energy.

The observation of the perforation-like structures causes the mind to speculate about how they initiate and how they evolve. Perhaps the micro-tunneling, which seems to have fostered the in-depth combustion process, may have encountered a physical inhomogeneity that directed and enlarged a crack along a fault line or plane. As the crack proceeded at high speed, ignition followed as the hot, high pressure gases rushed into the expanded volume. These proposed processes offer an explanation for the appearance of the several, very long, perforation-like tunnels. They also offer the possibility of directing the creation of perforation area through the introduction of intentional mechanical disturbances. Then, as the igniting plasma is injected, its energy could be tailored to make available surface area according to the pressure profile desired. Properly executed, this would provide optimum firing conditions over a wide range of applications. This could be done by using a specially made monolithic grain that would have incorporated within it mechanical stress flaws that provide programmed surface area upon demand. The term "virtual perforation" seems a proper descriptor for such a structure, since initially the perforation occupies no volume. The plasma may, under the proper conditions, interact with the virtual perforation and activate it to function as a perforation in a conventional multiperforated grain. This capability could provide significant advantages in several ways: by allowing multiple zoning from a single charge; by allowing several different types of projectiles to be used with the same charge; and by allowing the gun to always operate near its maximum permissible pressure, thereby reducing the weight of the gun for specific performance requirements.

Scallop formation was initially thought to be the result of the highly turbulent conditions that caused local erosive burning to carve a local depression. The discovery of in-depth burning adds another possible mechanism. The sharp line of demarcation between combusted and noncombusted

regions shown in Figure 9a provides evidence for another process. If this subsurface decomposition shown in that figure continues and spreads until deconsolidation of the combustion volume occurs, the remaining depression that is formed is similar in shape to the scallops observed in all residual grains.

Finally, the observance of no conventional thermal layer in some combustion surfaces (illustrated in Figure 18b) adds evidence for augmented mass generation by erosive burning or a similar micro-deconsolidation mechanism discussed previously. The dark band associated with this observation may be an indicator of some other process and warrants further investigation. Again, if such processes can be controlled, they can be used to control performance as the situation requires.

5. CONCLUSIONS

Evidence has been presented that indicates combustion processes in the 30-mm SPETC gun that do not occur to any significant degree in guns using conventional ignition systems. These processes include erosive burning, micro-deconsolidation, and in-depth combustion. Each process augments the mass generation rate of the propellant when compared to the rate expected from conventional external surface combustion.

The relative amount of augmented burning between erosive and tunneling mechanisms is likely to vary widely from grain to grain; the erosive component being determined by the plasma-forming parameters and the mechanical interaction of the plasma and the propellant surface. This should produce a repeatable and predictable augmentation to the normal burning. The tunneling process, as it is now perceived, is also dependent on the plasma formation parameters, but is strongly controlled by the extent and nature of mechanical inhomogeneities. If the grain has few flaws, then little area will be generated from this mode of plasma interaction. If many flaws exist, much more area can be created. Since JA2 is a thermoplastic, the production process includes an annealing cycle to relieve thermal stresses and promote material homogeneity. It seems as if the mass generation could be greatly enhanced by the proper placement of well designed virtual perforations.

Evidence is presented that demonstrates the nature of new surface area generation as a strong function of initial level of plasma-propellant interaction. Radial cracking, observed in early firings, was reduced by increasing circumferential confinement in the monolithic grains, while the degree of in-depth combustion increased with additional confinement. Tunneling, the mechanism through which virtual perforations may be used to produce controlled combustion surfaces, showed indications of control through the intentional introduction of mechanical inhomogeneities. This mechanism offers the possibility of a new process that could significantly augment mass generation and be of immense value if control can be demonstrated.

6. FUTURE STUDIES

More study is needed to characterize the SPETC combustion mechanisms and the methods to control them. The ongoing closed bomb work[12] needs to be completed. Once the measurement methods are more well understood, experiments to control the augmentation of mass generation should be performed using propellant with carefully introduced mechanical inhomogeneities. If a surface area profile can be produced that is a function of the electrical plasma generation parameters, then this method can be exploited to increase performance, reduce the number of required propelling charges, expand the gun's capability, and operate the weapon system near the optimal pressure at all times.

7. REFERENCES

1. L. Harris, D. Chiu, J. Prezelski, P. O'Reilly, R. Marchak, D. Downs, W. Oberle, J. Greig, H. McElroy, and J. Bezzett, "Enhanced Propellant Burn Rate Through Plasma Erosion," Proceedings of the 30th JANNAF Combustion Meeting, CPIA Publication 606, pp 121-135, November, 1993.

2. R. D. Anderson, and K. D. Fickie, "IBHVG2 — A Users Guide," BRL-TR-2829, Ballistic Research Laboratory, Aberdeen Proving Ground, MD, July 1987.

3. F. Robbins, Private Communication, Army Research Laboratory, Aberdeen Proving Ground, Maryland, 1994.

4. R.L. Derr, and T.L. Boggs, "Role of Scanning Electron Microscopy in the study of Solid Propellant Combustion: Part III. The Surface Structure and Profile Characteristics of Burning Composite Solid Propellants," *Combustion Science and Technology*, Volume 1, pp 369-284, 1970.

5. M.A. Schroeder, R.A. Fifer, M.S. Miller, R.A. Pesce-Rodriguez, and G. Singh, "Condensed-Phase Processes during Solid Propellant Combustion. II. Chemical and Microscopic Examination of Conductively Quenched Samples of RDX, XM39, JA2, M30, and HMX-Binder Compositions," Proceedings of the 27th JANNAF Combustion Meeting, CPIA Publication 557, Volume III, pp 99-114, November, 1990.

6. M.A. Schroeder, R.A. Fifer, M.S. Miller, R.A. Pesce-Rodriguez, C.J. Selawski, and G. Singh, "Condensed-Phase Processes during Solid Propellant Combustion. III. Some Preliminary Depth Profiling Studies on XM39, JA2, M9, and HMX2," Proceedings of the 28th JANNAF Combustion Meeting, CPIA Publication 573, Volume II, pp 541-552, October, 1991.

7. P. J. Kaste, J. Ceasar, and R. J. Lieb, "Scanning Electron Microscopy (SEM) to Probe Propellant Morphology," ARL-TR-230, Army Research Laboratory, Aberdeen Proving Ground, Maryland, October 1993.

8. R. J. Lieb, and M. G. Leadore, "Time-Temperature Shift Factors for Gun Propellants," ARL-TR-131, Army Research Laboratory, Aberdeen Proving Ground, Maryland, May 1993.

9. R. J. Lieb, and M. G. Leadore, "Mechanical Response Comparison of Gun Propellants Evaluated under Equivalent Time-Temperature Conditions," ARL-TR-228, Army Research Laboratory, Aberdeen Proving Ground, Maryland, September 1993.

10. R. Pesce-Rodriguez, Private Communication, Army Research Laboratory, Aberdeen Proving Ground, Maryland, 1994.

11. K. J. White, Private Communication, Army Research Laboratory, Aberdeen Proving Ground, Maryland, 1994.

12. W. F. Oberle, Private Communication, Army Research Laboratory, Aberdeen Proving Ground, Maryland, 1994.

Intentionally Left Blank

NO. OF COPIES	ORGANIZATION
2	ADMINISTRATOR DEFENSE TECHNICAL INFO CENTER ATTN: DTIC-DDA CAMERON STATION ALEXANDRIA VA 22304-6145
1	COMMANDER US ARMY MATERIEL COMMAND ATTN: AMCAM 5001 EISENHOWER AVE ALEXANDRIA VA 22333-0001
1	DIRECTOR US ARMY RESEARCH LABORATORY ATTN: AMSRL-OP-SD-TA/ RECORDS MANAGEMENT 2800 POWDER MILL RD ADELPHI MD 20783-1145
3	DIRECTOR US ARMY RESEARCH LABORATORY ATTN: AMSRL-OP-SD-TL/ TECHNICAL LIBRARY 2800 POWDER MILL RD ADELPHI MD 20783-1145
1	DIRECTOR US ARMY RESEARCH LABORATORY ATTN: AMSRL-OP-SD-TP/ TECH PUBLISHING BRANCH 2800 POWDER MILL RD ADELPHI MD 20783-1145
2	COMMANDER US ARMY ARDEC ATTN: SMCAR-TDC PICATINNY ARSENAL NJ 07806-5000
1	DIRECTOR BENET LABORATORIES ATTN: SMCAR-CCB-TL WATERVLIET NY 12189-4050
1	DIRECTOR US ARMY ADVANCED SYSTEMS RESEARCH AND ANALYSIS OFFICE ATTN: AMSAT-R-NR/MS 219-1 AMES RESEARCH CENTER MOFFETT FIELD CA 94035-1000

NO. OF COPIES	ORGANIZATION
1	COMMANDER US ARMY MISSILE COMMAND ATTN: AMSMI-RD-CS-R (DOC) REDSTONE ARSENAL AL 35898-5010
1	COMMANDER US ARMY TANK-AUTOMOTIVE COMMAND ATTN: AMSTA-JSK (ARMOR ENG BR) WARREN MI 48397-5000
1	DIRECTOR US ARMY TRADOC ANALYSIS COMMAND ATTN: ATRC-WSR WSMR NM 88002-5502
1	COMMANDANT US ARMY INFANTRY SCHOOL ATTN: ATSH-WCB-O FORT BENNING GA 31905-5000
	ABERDEEN PROVING GROUND
2	DIR, USAMSAA ATTN: AMXSY-D AMXSY-MP/H COHEN
1	CDR, USATECOM ATTN: AMSTE-TC
1	DIR, USAERDEC ATTN: SCBRD-RT
1	CDR, USACBDCOM ATTN: AMSCB-CII
1	DIR, USARL ATTN: AMSRL-SL-I
5	DIR, USARL ATTN: AMSRL-OP-AP-L

No. of
Copies Organization

1 HQDA (SARD-TR/Ms. K. Kominos)
WASH DC 20310-0103

1 HQDA (SARD-TR/Dr. R.Chait)
WASH DC 20310-0103

1 Chairman
DOD Explosives Safety Board
Room 856-C
Hoffman Bldg. 1
2461 Eisenhower Avenue
Alexandria, VA 22331-0600

1 Headquarters
U.S. Army Materiel Command
ATTN: AMCDCG-T, M. Fisette
5001 Eisenhower Ave.
Alexandria, VA 22333-0001

1 U.S. Army Ballistic Missile
Defense Systems Command
Advanced Technology Center
P.O. Box 1500
Huntsville, AL 35807-3801

1 Department of the Army
Office of the Product Manager
155mm Howitzer, M109A6, Paladin
ATTN: SFAE-AR-HIP-IP,
Mr. R. De Kleine
Picatinny Arsenal, NJ 07806-5000

3 Project Manager
Advanced Field Artillery System
ATTN: SFAE-ASM-AF-E,
LTC A. Ellis
T. Kuriata
J. Shields
Picatinny Arsenal, NJ 07801-5000

1 Project Manager
Advanced Field Artillery System
ATTN: SFAE-ASM-AF-Q, W. Warren
Picatinny Arsenal, NJ 07801-5000

1 Commander
Production Base Modernization Agency
U.S. Army Armament Research,
Development, and Engineering Center
ATTN: AMSMC-PBM, A. Siklosi
Picatinny Arsenal, NJ 07806-5000

No. of
Copies Organization

1 Commander
Production Base Modernization Agency
U.S. Army Armament Research,
Development, and Engineering Center
ATTN: AMSMC-PBM-E, L. Laibson
Picatinny Arsenal, NJ 07806-5000

1 PEO-Armaments
Project Manager
Tank Main Armament System
ATTN: AMCPM-TMA
Picatinny Arsenal, NJ 07806-5000

1 PEO-Armaments
Project Manager
Tank Main Armament System
ATTN: AMCPM-TMA-105
Picatinny Arsenal, NJ 07806-5000

1 PEO-Armaments
Project Manager
Tank Main Armament System
ATTN: AMCPM-TMA-120
Picatinny Arsenal, NJ 07806-5000

1 PEO-Armaments
Project Manager
Tank Main Armament System
ATTN: AMCPM-TMA-AS, H. Yuen
Picatinny Arsenal, NJ 07806-5000

3 Commander
U.S. Army Armament Research,
Development, and Engineering Center
ATTN: SMCAR-CCH-V,
C. Mandala
E. Fennell
F. Hildebrant
Picatinny Arsenal, NJ 07806-5000

1 Commander
U.S. Army Armament Research,
Development, and Engineering Center
ATTN: SMCAR-CCH-T, L. Rosendorf
Picatinny Arsenal, NJ 07806-5000

1 Commander
U.S. Army Armament Research,
Development, and Engineering Center
ATTN: SMCAR-CCS
Picatinny Arsenal, NJ 07806-5000

No. of
Copies Organization

1 Commander
U.S. Army Armament Research,
Development, and Engineering Center
ATTN: SMCAR-AEE, J. Lannon
Picatinny Arsenal, NJ 07806-5000

13 Commander
U.S. Army Armament Research,
Development, and Engineering Center
ATTN: SMCAR-AEE-B,
A. Beardell
D. Downs
S. Einstein
S. Westley
S. Bernstein
J. Rutkowski
B. Brodman
P. O'Reilly
R. Cirincione
P. Hui
J. O'Reilly
B. Strauss
J. Prezelski
Picatinny Arsenal, NJ 07806-5000

5 Commander
U.S. Army Armament Research,
Development, and Engineering Center
ATTN: SMCAR-AEE-WW,
M. Mezger
J. Pinto
D. Wiegand
P. Lu
C. Hu
Picatinny Arsenal, NJ 07806-5000

1 Commander
U.S. Army Armament Research,
Development, and Engineering Center
ATTN: SMCAR-AES, S. Kaplowitz
Picatinny Arsenal, NJ 07806-5000

1 Commander
U.S. Army Armament Research,
Development and Engineering Center
ATTN: SMCAR-HFM, E. Barrieres
Picatinny Arsenal, NJ 07806-5000

1 Commander
U.S. Army Armament Research,
Development and Engineering Center
ATTN: AMSMC-PBE, D. Fair
Picatinny Arsenal, NJ 07806-5000

No. of
Copies Organization

1 Commander
U.S. Army Armament Research,
Development and Engineering Center
ATTN: SMCAR-FSA-F, LTC R. Riddle
Picatinny Arsenal, NJ 07806-5000

1 Commander
U.S. Army Armament Research,
Development and Engineering Center
ATTN: SMCAR-FSC, G. Ferdinand
Picatinny Arsenal, NJ 07806-5000

1 Commander
U.S. Army Armament Research,
Development and Engineering Center
ATTN: SMCAR-FS, T. Gora
Picatinny Arsenal, NJ 07806-5000

1 Commander
U.S. Army Armament Research,
Development and Engineering Center
ATTN: SMCAR-FS-DH, J. Feneck
Picatinny Arsenal, NJ 07806-5000

3 Commander
U.S. Army Armament Research,
Development and Engineering Center
ATTN: SMCAR-FSS-A,
R. Kopmann
B. Machek
L. Pinder
Picatinny Arsenal, NJ 07806-5000

1 Commander
U.S. Army Armament Research,
Development and Engineering Center
ATTN: SMCAR-FSN-N, K. Chung
Picatinny Arsenal, NJ 07806-5000

3 Director
US Army Benet Laboratory
ATTN: SMCAR-CCB-RA,
G.P. O'Hara
G.A. Pflegl
SMCAR-CCB-S, F. Heiser
Watervliet, NY 12189-4050

1 Director
Benet Laboratories
ATTN: SMCAR-CCB-R Sam Sopok
Watervliet, NY 12189-4050

No. of
Copies Organization

3 Commander
U.S. Army Research Office
ATTN: Technical Library
D. Mann
Mr. K. Clark
P.O. Box 12211
Research Triangle Park, NC 27709-2211

1 Commander, USACECOM
R&D Technical Library
ATTN: ASQNC-ELC-IS-L-R,
Myer Center
Fort Monmouth, NJ 07703-5301

1 Commandant
U.S. Army Aviation School
ATTN: Aviation Agency
Fort Rucker, AL 36360

1 Program Manager
U.S. Tank-Automotive Command
ATTN: AMCPM-ABMS, T. Dean
Warren, MI 48092-2498

1 Project Manager
U.S. Tank-Automotive Command
Fighting Vehicle Systems
ATTN: SFAE-ASM-BV
Warren, MI 48397-5000

1 Project Manager, Abrams Tank System
ATTN: SFAE-ASM-AB
Warren, MI 48397-5000

1 Director
HQ, TRAC RPD
ATTN: ATCD-MA
Fort Monroe, VA 23651-5143

1 Commander
U.S. Army Belvoir Research and
Development Center
ATTN: STRBE-WC
Fort Belvoir, VA 22060-5006

1 Director
U.S. Army TRAC-Ft. Lee
ATTN: ATRC-L, Mr. Cameron
Fort Lee, VA 23801-6140

1 Commandant
U.S. Army Command and General
Staff College
Fort Leavenworth, KS 66027

No. of
Copies Organization

1 Commandant
U.S. Army Special Warfare School
ATTN: Rev and Trng Lit Div
Fort Bragg, NC 28307

1 Commander
Radford Army Ammunition Plant
ATTN: SMCAR-QA/HI LIB
Radford, VA 24141-0298

1 Commander
U.S. Army Foreign Science and
Technology Center
ATTN: AMXST-MC-3
220 Seventh Street, NE
Charlottesville, VA 22901-5396

2 Commandant
U.S. Army Field Artillery Center and
School
ATTN: ATSF-CO-MW, E. Dublisky
ATSF-CN, P. Gross
Ft. Sill, OK 73503-5600

1 Commandant
U.S. Army Armor School
ATTN: ATZK-CD-MS, M. Falkovitch
Armor Agency
Fort Knox, KY 40121-5215

2 U.S. Army Research Development and
Standardization Group (UK)
ATTN: Dr. Roy E. Richenbach
Heinrich Egghart
PSC 802 Box 15,
FPO AE 09499-1500

2 Commander
Naval Sea Systems Command
ATTN: SEA 62R
SEA 64
Washington, DC 20362-5101

1 Commander
Naval Sea System Command
Code: 91WM
ATTN: Mr. John Delany
Arlington, VA 22242-5160

1 Commander
Naval Air Systems Command
ATTN: AIR-954-Tech Library
Washington, DC 20360

No. of
Copies Organization

4 Commander
Naval Research Laboratory
ATTN: Technical Library
Code 4410,
K. Kailasanate
J. Boris
E. Oran
Washington, DC 20375-5000

1 Office of Naval Research
ATTN: Code 473, R.S. Miller
800 N. Quincy Street
Arlington, VA 22217-9999

1 Commander
US Naval Surface Warfare Center
ATTN: S. Culder, Code 290D
Bldg. 600
Indian Head, MD 20640-5000

1 Office of Naval Technology
ATTN: ONT-213, D. Siegel
800 N. Quincy St.
Arlington, VA 22217-5000

3 Commander
Naval Surface Warfare Center
ATTN: Code 730
Code R-13
R. Bernecker, Code R-10
Silver Spring, MD 20903-5000

8 Commander
Naval Surface Warfare Center
ATTN: T.C. Smith
K. Rice
S. Mitchell
S. Peters, Code 6210C
J. Consaga
C. Gotzmer
R. Simmons, Code 210PI
Technical Library
Indian Head, MD 20640-5000

4 Commander
Naval Surface Warfare Center
ATTN: Code G30, Guns & Munitions Div
Code G32, Guns Systems Div
Code G33, T. Doran
Code E23 Technical Library
Dahlgren, VA 22448-5000

No. of
Copies Organization

5 Commander
Naval Air Warfare Center
ATTN: Code 388,
C.F. Price
T. Boggs
Code 3895,
T. Parr
R. Derr
Information Science Division
China Lake, CA 93555-6001

1 Commanding Officer
Naval Underwater Systems Center
ATTN: Code 5B331, Technical Library
Newport, RI 02840

1 AFOSR/NA
ATTN: J. Tishkoff
Bolling AFB, D.C. 20332-6448

1 OLAC PL/TSTL
ATTN: D. Shiplett
Edwards AFB, CA 93523-5000

3 OL-AC PL/RK
ATTN: J. Levine
L. Quinn
T. Edwards
5 Pollux Drive
Edwards AFB, CA 93524-7048

1 WL/MNAA
ATTN: B. Simpson
Eglin AFB, FL 32542-5434

1 WL/MNME
Energetic Materials Branch
2306 Perimeter Rd.
STE 9
Eglin AFB, FL 32542-5910

1 WL/MNSH
ATTN: R. Drabczuk
Eglin AFB, FL 32542-5434

No. of
Copies Organization

1 Central Intelligence Agency
Office of Information Resources
Room GA-07, HQS
Washington, DC 20505

1 Central Intelligence Agency
ATTN: J. Backofen
NHB, Room 5N01
Washington, DC 20505

1 SDIO/TNI
ATTN: L.H. Caveny
Pentagon
Washington, DC 20301-7100

1 SDIO/DA
ATTN: E. Gerry
Pentagon
Washington, DC 21301-7100

2 HQ DNA
ATTN: D. Lewis
A. Fahey
6801 Telegraph Rd.
Alexandria, VA 22310-3398

1 Director
Sandia National Laboratories
Energetic Materials & Fluid Mechanics
Department, 1512
ATTN: M. Baer
P.O. Box 5800
Albuquerque, NM 87185

1 Director
Sandia National Laboratories
Combustion Research Facility
ATTN: R. Carling
Livermore, CA 94551-0469

1 Director
Sandia National Laboratories
ATTN: 8741, G. A. Beneditti
P.O. Box 969
Livermore, CA 94551-0969

2 Director
Lawrence Livermore National
Laboratory
ATTN: L-355,
A. Buckingham
M. Finger
P.O. Box 808
Livermore, CA 94550-0622

No. of
Copies Organization

2 Director
Los Alamos Scientific Lab
ATTN: T3/D. Butler
M. Division/B. Craig
P.O. Box 1663
Los Alamos, NM 87544

2 CPIA - JHU
ATTN: H. J. Hoffman
T. Christian
10630 Little Patuxent Parkway
Suite 202
Columbia, MD 21044-3200

1 Brigham Young University
Department of Chemical Engineering
ATTN: M. Beckstead
Provo, UT 84601

1 Jet Propulsion Laboratory
California Institute of Technology
ATTN: L.D. Strand, MS 125/224
4800 Oak Grove Drive
Pasadena, CA 91109

1 California Institute of Technology
204 Karman Lab
Main Stop 301-46
ATTN: F.E.C. Culick
1201 E. California Street
Pasadena, CA 91109

3 Georgia Institute of Technology
School of Aerospace Engineering
ATTN: B.T. Zim
E. Price
W.C. Strahle
Atlanta, GA 30332

2 University of Illinois
Department of Mechanical/Industry
Engineering
ATTN: H. Krier
R. Beddini
144 MEB; 1206 N. Green St.
Urbana, IL 61801-2978

1 University of Massachusetts
Department of Mechanical Engineering
ATTN: K. Jakus
Amherst, MA 01002-0014

No. of
Copies Organization

1 University of Minnesota
Department of Mechanical Engineering
ATTN: E. Fletcher
Minneapolis, MN 55414-3368

5 Pennsylvania State University
Department of Mechanical Engineering
ATTN: V. Yang
K. Kuo
Wen H. Hsieh
Stefan T. Thynell
C. Merkle
University Park, PA 16802-7501

1 Rensselaer Polytechnic Institute
Department of Mathematics
Troy, NY 12181

1 Stevens Institute of Technology
Davidson Laboratory
ATTN: R. McAlevy III
Castle Point Station
Hoboken, NJ 07030-5907

1 Stevens Institute of Technology
Highly Filled Materials Institute
ATTN: Dr. Dilhan M. Kaylon
Hoboken, NJ 07030

1 Rutgers University
Department of Mechanical and
Aerospace Engineering
ATTN: S. Temkin
University Heights Campus
New Brunswick, NJ 08903

1 University of Utah
Department of Chemical Engineering
ATTN: A. Baer
Salt Lake City, UT 84112-1194

1 Washington State University
Department of Mechanical Engineering
ATTN: C.T. Crowe
Pullman, WA 99163-5201

1 3M Specialty Chemicals
ATTN: A. P. Manzara
Bldg 70-2
10746 Chemolite Road
Cottage Grove, MN 55016

No. of
Copies Organization

2 Battelle
ATTN: TWSTIAC
V. Levin
505 King Avenue
Columbus, OH 43201-2693

1 Battelle PNL
ATTN: M.C.C. Bampton
P.O. Box 999
Richland, WA 99352

1 E. I. Du Pont De Nemours & Co, .Inc.
Potomac River Works,
ATTN: M. McGowan
Martinsburg, WV 25401

1 Eli Freedman & Associates
2411 Diana Road
Baltimore, MD 21209

1 Institute of Gas Technology
ATTN: D. Gidaspow
3424 S. State Street
Chicago, IL 60616-3896

1 Institute for Advanced Technology
ATTN: T.M. Kiehne
The University of Texas of Austin
4030-2 W. Braker Lane
Austin, TX 78759-5329

1 AFELM, The Rand Corporation
ATTN: Library D
1700 Main Street
Santa Monica, CA 90401-3297

1 Arrow Technology Associates, Inc.
ATTN: W. Hathaway
P.O. Box 4218
South Burlington, VT 05401-0042

2 AAI Corporation
ATTN: J. Frankle
D. Cleveland
P.O. Box 126
Hunt Valley, MD 21030-0126

2 Alliant Techsystems, Inc.
ATTN: R.E. Tompkins
J. Kennedy
7225 Northland Dr.
Brooklyn Park, MN 55428

No. of
Copies Organization

6 Alliant Techsystems
ATTN: J. Bode
C. Candland
L. Osgood
R. Buretta
R. Becker
M. Swenson
600 Second St NE
Hopkins, MN 55343

1 Textron Defense Systems
ATTN: A. Patrick
2385 Revere Beach Parkway
Everett, MA 02149-5900

1 General Applied Sciences Lab
ATTN: J. Erdos
77 Raynor Ave.
Ronkonkama, NY 11779-6649

1 General Electric Company
Tactical System Department
ATTN: J. Mandzy
100 Plastics Ave.
Pittsfield, MA 01201-3698

1 IITRI
ATTN: M.J. Klein
10 W. 35th Street
Chicago, IL 60616-3799

5 Hercules, Inc.
Radford Army Ammunition Plant
ATTN: L. Gizzi
D.A. Worrell
W.J. Worrell
C. Chandler
F. T. Kristoff
Radford, VA 24141-0299

2 Hercules, Inc.
Allegheny Ballistics Laboratory
ATTN: William B. Walkup
Thomas F. Farabaugh
P.O. Box 210
Rocket Center, WV 26726

1 Hercules, Inc.
ATTN: D. D. Whitney
100 Howard Blvd.
Kenvil, NJ 07847

No. of
Copies Organization

1 Hercules, Inc.
Hercules Plaza
ATTN: B.M. Riggleman
Wilmington, DE 19894

1 Hercules, Inc.
ATTN: E. Hays Zeigler
Kenvil, NJ 07847

1 MBR Research Inc.
ATTN: Dr. Moshe Ben-Reuven
601 Ewing St., Suite C-22
Princeton, NJ 08540

1 Olin Corporation
Badger Army Ammunition Plant
ATTN: F.E. Wolf
Baraboo, WI 53913

3 Olin Ordnance
ATTN: E.J. Kirschke
A.F. Gonzalez
D.W. Worthington
P.O. Box 222
St. Marks, FL 32355-0222

1 Olin Ordnance
ATTN: H.A. McElroy
10101 9th Street, North
St. Petersburg, FL 33716

1 Paul Gough Associates, Inc.
ATTN: P.S. Gough
1048 South St.
Portsmouth, NH 03801-5423

1 Physics International Library
ATTN: H. Wayne Wampler
P.O. Box 5010
San Leandro, CA 94577-0599

2 Princeton Combustion Research
Laboratories, Inc.
ATTN: N. Mer
N.A. Messina
Princeton Corporate Plaza
11 Deerpark Dr., Bldg IV, Suite 119
Monmouth Junction, NJ 08852

2 Rockwell International
Rocketdyne Division
ATTN: BA05, J. Flanagan
WC79, R. Edelman
6633 Canoga Avenue
Canoga Park, CA 91303-2703

No. of
Copies Organization

2 Rockwell International Science Center
ATTN: Dr. S. Chakravarthy
Dr. S. Palaniswamy
1049 Camino Dos Rios
P.O. Box 1085
Thousand Oaks, CA 91360

1 Southwest Research Institute
ATTN: J.P. Riegel
6220 Culebra Road
P.O. Drawer 28510
San Antonio, TX 78228-0510

1 Thiokol Corporation
Elkton Division
ATTN: Tech Library
P.O. Box 241
Elkton, MD 21921-0241

1 Thiokol Corp.
ATTN: Dr. David A. Flanigan
PO Box 707
Brigham City, UT 84302-0707

No. of
Copies Organization

1 Thiokol Corp.
Tactical Operations
ATTN: W. H. Oetjen
PO Box 400006
Huntsville, AL 35815-1506

1 Veritay Technology, Inc.
ATTN: E. Fisher
4845 Millersport Hwy.
East Amherst, NY 14501-0305

1 Universal Propulsion Company
ATTN: H.J. McSpadden
25401 North Central Ave.
Phoenix, AZ 85027-7837

1 SRI International
Propulsion Sciences Division
ATTN: Tech Library
333 Ravenwood Avenue
Menlo Park, CA 94025-3493

Aberdeen Proving Ground

1 Cdr, USACSTA
ATTN: STECS-LI, R. Hendricksen

No. of
Copies Organization

1 Ernst-Mach-Institut
ATTN: Dr. G. Zimmerman
Haupstrasse 18
Weil am Rheim
Germany

1 Defence Research Agency, Military Division
ATTN: Dr. D. Tod
Room 20, Bld. X50, ET5
Fort Halstead
Sevenoaks, Kent, TN14 7BP
England

1 School of Mechanical, Materials, and Civil Engineering
ATTN: Dr. Bryan Lawton
Royal Military College of Science
Shrivenham, Swindon, Wiltshire, SN6 8LA
England

1 Prins Maurits Laboratorium
ATTN: Mr. Jan Miedema
P.O. Box 45
2280 AA Rijswijk ZH
The Netherlands

1 Etablissement Technique de Bourges (ETBS)
LPI (Division Laboratoires Matemiaux Pyrotechniques et Inertes)
BP n°712
ATTN: Mr. Alain Fabre
18015 Bourges CEDEX
France

No. of
Copies Organization

1 SNPE Centre de Recherches du Bouchet
ATTN: Mr. Robert Nevière
BP2 91710 Vert-le-Petit
France

2 Institut Saint Louis
ATTN: Dr. Marc Giraud
Dr. Gunther Sheets
Postfach 1260
7858 Weil am Rhein 1
Germany

1 Explosive Ordnance Division
ATTN: A. Wildegger-Gaissmaier
Defence Science and Technology Organisation
P.O. Box 1750
Salisbury, South Australia 5108

1 Chief
Defence Research Establishment Valcartier
ATTN: Dr. S. Duncan
P.O. Box 8800
Courcelette, Quebec G0A 1R0
Canada

1 BICT
ATTN: Dr. Burkhard Nicklas
Grosse Cent
D-53913 Swisttal 1
Germany

USER EVALUATION SHEET/CHANGE OF ADDRESS

This Laboratory undertakes a continuing effort to improve the quality of the reports it publishes. Your comments/answers to the items/questions below will aid us in our efforts.

1. ARL Report Number ARL-TR-606 Date of Report November 1994

2. Date Report Received _____

3. Does this report satisfy a need? (Comment on purpose, related project, or other area of interest for which the report will be used.) _____

4. Specifically, how is the report being used? (Information source, design data, procedure, source of ideas, etc.) _____

5. Has the information in this report led to any quantitative savings as far as man-hours or dollars saved, operating costs avoided, or efficiencies achieved, etc? If so, please elaborate. _____

6. General Comments. What do you think should be changed to improve future reports? (Indicate changes to organization, technical content, format, etc.) _____

CURRENT ADDRESS

_____
Organization

_____
Name

_____
Street or P.O. Box No.

_____
City, State, Zip Code

7. If indicating a Change of Address or Address Correction, please provide the Current or Correct address above and the Old or Incorrect address below.

OLD ADDRESS

_____
Organization

_____
Name

_____
Street or P.O. Box No.

_____
City, State, Zip Code

(Remove this sheet, fold as indicated, tape closed, and mail.)
(DO NOT STAPLE)